Mixing and segregation of granular materials in chute flows

D. V. Khakhar
Department of Chemical Engineering, Indian Institute of Technology—Bombay, Powai, Mumbai 400076, India

J. J. McCarthy
Department of Chemical Engineering, University of Pittsburgh, Pittsburgh, Pennsylvania 15261

J. M. Ottino[a)]
Department of Chemical Engineering, Northwestern University, Evanston, Illinois 60208

(Received 27 January 1999; accepted for publication 4 May 1999)

Mixing of granular solids is invariably accompanied by segregation, however, the fundamentals of the process are not well understood. We analyze density and size segregation in a chute flow of cohesionless spherical particles by means of computations and theory based on the transport equations for a mixture of nearly elastic particles. Computations for elastic particles (Monte Carlo simulations), nearly elastic particles, and inelastic, frictional particles (particle dynamics simulations) are carried out. General expressions for the segregation fluxes due to pressure gradients and temperature gradients are derived. Simplified equations are obtained for the limiting cases of low volume fractions (ideal gas limit) and equal sized particles. Theoretical predictions of equilibrium number density profiles are in good agreement with computations for mixtures of equal sized particles with different density for all solids volume fractions, and for mixtures of different sized particles at low volume fractions ($\nu<0.2$), when the particles are elastic or nearly elastic. In the case of inelastic, frictional particles the theory gives reasonable predictions if an appropriate effective granular temperature is assumed. The relative importance of pressure diffusion and temperature diffusion for the cases considered is discussed. © *1999 American Institute of Physics.* [S1054-1500(99)01603-1]

An important industrial and fundamental problem is the tendency for granular mixtures to demix or segregate. Small differences in either size or density of the particles lead to *flow-induced segregation*. The fundamentals of the process are, in general, imperfectly understood. Constitutive equations for the case of equal size/different density particle systems have been proposed; the case of equal density/different size particles is more complex. We analyze density and size segregation of cohesionless spherical particles in the simplest possible flow—a chute flow—by means of computations and theory based on the transport equations for a mixture of nearly elastic particles. Simplified equations are possible for limiting cases; e.g. low volume fractions, equal sized particles. The results are important in continuum modeling descriptions of mixing and segregation of granular flows.

I. INTRODUCTION

Mixing of granular materials is invariably accompanied by segregation-driven-processes resulting from differences in size, density, shape, roughness, etc., of the constituents of the mixture. While a qualitative understanding of the mechanisms of segregation has existed for some time now,[1–3] there are remarkably few models—especially simple one—which give quantitative predictions of the extent of segregation and that can be used in conjunction with other modeling tools. Such information is particularly important in the analysis and design of industrial mixing operations in the pharmaceutical, chemical, food, ceramic, and construction industries. Current practices are empirical with limited possibilities of generalization. The design of mixers, for example, is based on heuristics arrived at by prior experience. The lack of general constitutive equations to predict the extent of segregation is clearly a hindrance to systematic approaches to the problem.

Several previous studies of granular segregation have focused on chute flows[4–7]—continuous flows of granular material in inclined channels. Besides the practical importance of such flows in granular transportation, the simplicity of the flows allows for detailed development and testing of theory. Further, the results from such studies can be applied to other systems involving free surface flows (where much of the segregation takes place) such as drum mixers, rotary kilns, and the formation of heaps of granular materials. We review studies of segregation both in chute flows and in other free surface flows below.

Particle dynamics simulations (PDS), in which properties of particles such as size, shape, and density can be directly specified, appear to be the most suitable tools for analyzing segregation.[8] Details such as velocity and concentration profiles for every component in a mixture can be obtained. Physical insight does not necessarily follow; the results are only as useful as those resulting from well-designed experiments. Moreover, computational intensity typically limits such simulations to relatively small systems

[a)]Electronic mail: ottino@chem-eng.nwu.edu

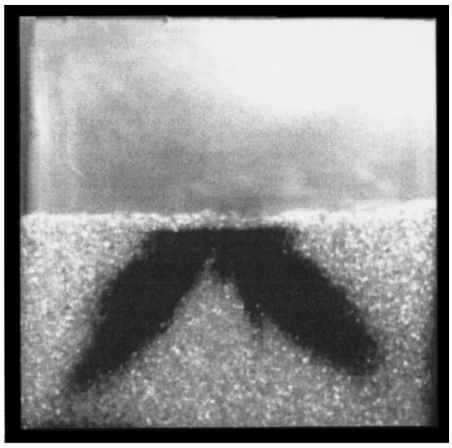

FIG. 1. Segregated pattern formed by rotation of a mixture of different sized particles in a partially filled square mixer (Ref. 13).

(less than 10^4 particles) and to simple particle shapes (spheres, spheroids, and fused spheres). Recent results[9] also indicate sensitivity of the results of PDS to particle properties. In contrast, continuum theories do not have the limitations of scale-up to larger system sizes. These models are based on constitutive relations obtained by fitting phenomenological equations to various data, such as PDS simulations, or analyses based on statistical mechanics for simple geometries (spheres) and nearly elastic particles. Often, however, physical insight is required in order to simplify the equations to a tractable form.

Transport equations obtained using kinetic theory for slightly inelastic spheres in rapid flow (no sustained contacts between particles) are analogous to those for fluids.[10] The *granular temperature*, defined as a quantity proportional to the average kinetic energy of a particle associated with fluctuations (i.e., the mean kinetic energy per particle less the kinetic energy of a particle moving at the mean velocity in the averaging volume), plays an important role. Since collisions dissipate energy, a constant source of work is required to sustain the fluidity of the granular material. Continuum theories broadly based on this approach, in some cases including empirical corrections for interparticle friction, have been successful in predicting experimentally measured stresses and flow profiles for beads in shear flows and chute flows.[11,12] Surprisingly, continuum models are found to work in many cases, even for flowing layers only a few diameters thick.

Continuum theory presents a complementary tool for the analysis of segregation. Moreover, continuum theories are ideally suited to investigate the competition between mixing and segregation, a topic that should be of interest to the readers of this journal, given the rich interplay between chaotic advection on one hand, and segregation-induced demixing on the other. Figure 1 shows a typical example of this in which steel balls and glass beads of equal size are rotated in a square mixer.[13] The equilibrium pattern reflects the underlying Poincaré section for the flow and a continuum model utilizing segregation flux expressions derived in this work predicts the pattern formed.

The main objective of the present work is to gain an understanding of the factors affecting the segregation of mixtures of cohesionless spherical particles in chute flows, and thus to develop simple continuum models for calculating segregation fluxes. The effect of differences in size and density are considered by means of computations involving an increasing level of detail. Monte Carlo simulations, in which the system is isothermal and the particles are elastic and frictionless, correspond to the simplest case. Particle dynamics simulations of inelastic frictionless particles represent the next level of detail, and particle dynamics simulations with realistic frictional and collisional interactions between particles are the closest to the actual system. The results of the simulation are compared to the predictions of the kinetic theory with the goal of testing the limits of applicability of the theory with respect to size and density segregation.

The paper is organized as follows. Section II reviews theoretical studies related to segregation in granular flows and Sec. III reviews the kinetic theory equations for a binary mixture of spherical particles. Governing equations for diffusion and segregation are obtained for two cases: (i) elastic particles at a uniform temperature in a gravitational field and (ii) inelastic particles in a chute flow. Section IV gives the details of the computational procedures whereas the computational results and comparison to theory are presented in Sec. V. Section VI gives the summary and conclusions.

II. SEGREGATION MODELS

Savage and Lun[4] presented the first detailed model for segregation due to size differences in a chute flow based on a *percolation* mechanism. The net percolation flux of the smaller particles in the direction of the gravitational component normal to the flowing layer was obtained by statistical analysis. The analysis was based on the assumption that in a dense flowing layer small voids are more likely to be formed than larger ones. Thus, smaller particles drop into voids with a greater frequency as compared to larger particles, resulting in a larger downward flux of the smaller particles. The reverse flux, which results from the requirement of maintaining a zero total flux of particles normal to the layer, is the same for both types of particles. The net result is a downward flux of the smaller particles and an upward flux of the larger particles resulting in segregation. The distribution of void sizes is obtained by considering simple arrangements of particles in a layer, and the frequency of dropping is obtained from dimensional analysis. Comparisons of the distance along the chute at which the material segregates completely into two layers is found to be in agreement with experiments for chute flow of mixtures of polystyrene beads of different sizes.

Dolgunin and co-workers[6,7] proposed simple phenomenological equations for the segregation flux resulting from density or size differences. The flux is assumed to depend on the concentration of the particles and the granular temperature. The segregation flux is balanced by mixing due to particle collisional diffusion resulting in an equilibrium distribution of particles across the flowing layer. The theory predicts s-shaped concentration profiles at equilibrium that are in agreement with experimentally obtained profiles. The model, however, is not rigorous and thus does not clearly

specify the driving forces for the segregation or the dependence of the segregation flux on the particle properties.

In a previous work[14] we obtained a constitutive equation for the segregation flux for a mixture of equal sized but different density spheres using an effective medium approach. The segregation flux is assumed to be proportional to the buoyant force acting on a particle immersed in an effective medium of the density of the mixture surrounding it. The denser particles thus sink to lower positions in the flowing layer, and the driving force for segregation in this case is the pressure gradient across the layer. This simple idea works quite well. Predictions of the equilibrium number density profile for the particle mixture in a gravitational field are in good agreement with computational results obtained from Monte Carlo simulations (elastic, frictionless spheres) and particle dynamics simulations for chute flow (inelastic, frictional spheres). The segregation flux when incorporated into a model for flow and diffusion in a rotating cylinder, also gave good agreement with the distribution of particles obtained from *radial segregation* of a mixture of steel and glass balls. In this case the denser particles sink to lower positions of the flowing layer, and thus are incorporated into an inner radial core, whereas the lighter glass particles are at the periphery. This is an example of the end use of constitutive models such as the one developed in this work. The case of size segregation requires a more complex description than that for density segregation, as shown below.

The early work of Nityanand *et al.*[15] experimentally illustrates the behavior of size segregation. At low rotational speeds of the cylinder, percolation (the Savage and Lun[4] mechanism discussed above) dominates and the smaller particles sink to lower levels in the flowing layer, which results in the formation of a core of the smaller particles. However, at higher rotational speeds the segregation pattern reverses with the smaller particles at the periphery instead of the core. These results have not been previously explained. Recent studies of radial segregation have focused primarily on the low rotational speed regime.[16–20] Baumann *et al.*[19] suggested a trapping mechanism for size segregation, and more recently Prigozhin and Kalman[20] have proposed a method for estimation of radial segregation based on measurements taken in heap formation.

While the theories for segregation reviewed above provide some physical insight into the process, only a few are grounded on fundamentals. The statistical mechanical studies of hard sphere mixtures provide a starting point for the understanding of granular segregation, and these results form the core of the current work. The most complete kinetic theory for multicomponent mixtures of hard spheres is given by de Haro *et al.*[21] Kincaid *et al.*[22] computed thermal diffusion factors (α_{ij}) defined as

$$\alpha_{ij}\nabla \ln T = \nabla \ln(n_j/n_i) \tag{1}$$

to characterize the segregation in the system due to temperature gradients. Here n_i is the number density of species i and T is the temperature, and the thermal diffusion factor gives the magnitude and direction of the segregation relative to the temperature gradient. Jenkins and Mancini[23] showed that the equations derived by de Haro *et al.*[21] are valid to the first order of approximation for slightly inelastic spheres. Application of these equations for analysis of granular segregation is limited. Arnarson and Willits[24] used the equations to compute the thermal diffusion factors defined above for binary mixtures taking into account both granular temperature and pressure gradients in one spatial direction. Computational results are presented to map out regions of the parameter space (size ratio, density ratio, solids volume fraction, number fraction, and the ratio of the pressure gradient normalized by the number density to the temperature gradient) in which α_{AB} is positive or negative. The only previous study of segregation in a granular flow based on the kinetic theory equations appears to be that of Hsiau and Hunt,[5] who considered the shear flow of a mixture of different sized particles. The gradient in temperature results in the particles migrating to the higher velocity and thus higher temperature regions. Such temperature-induced segregation in a chute flow would undoubtedly result in some of the smaller particles migrating to the top of the layer; this is the reverse of the predictions of Savage and Lun[4] and experimental results.[4,6,7] Gravitational effects were not considered in the study. In contrast, the two-dimensional numerical study of Hirschfield and Rappaport[25] for Lennard-Jones particles in a chute flow under gravity showed that large particles rise to the top of the layer. The studies were carried out for a few large particles in a large number of small particles.

The works reviewed above indicate that qualitatively different results for segregation may be obtained depending on the driving forces and the regime of operation. We discuss a general theory that encompasses these different effects in Secs. III.

III. THEORY

Here we briefly review the transport equations for a binary mixture of slightly inelastic spheres. The equations are given in Jenkins and Mancini,[23] however, we reproduce them below for completeness. The application to specific cases is considered next.

Consider a binary mixture of spherical particles of masses m_1 and m_2, and radii R_1 and R_2. The species balance equation is given by

$$\frac{\partial \rho_i}{\partial t} + \nabla \cdot (\rho_i \mathbf{u}_i) = 0, \quad i = 1,2, \tag{2}$$

where $\rho_i = n_i m_i$ is the mass density of species i, n_i is the number density of i, and $\mathbf{u}_i$ is the average velocity of i. The linear momentum balance equation is given by

$$\rho\left(\frac{\partial \mathbf{u}}{\partial t} + \mathbf{u}\cdot\nabla\mathbf{u}\right) = \nabla\cdot\mathbf{P} + \rho\mathbf{g}, \tag{3}$$

where $\rho = (\rho_1 + \rho_2)$ is the density of the mixture, $\mathbf{u} = (\rho_1\mathbf{u}_1 + \rho_2\mathbf{u}_2)$ is the mass averaged velocity, $\mathbf{P}$ is the stress, and $\mathbf{g}$ the acceleration due to gravity. The stress is written as $\mathbf{P} = -p\mathbf{I} - \tau$, where the granular pressure (p) is the isotropic part, and the deviatoric part τ depends on the local velocity gradient. Finally, the energy balance equation in terms of the granular temperature (T) is given by

$$n\left(\frac{\partial T}{\partial t}+\mathbf{u}\cdot\nabla T\right)=T\nabla\cdot\mathbf{J}_t-\nabla\cdot\mathbf{q}+\mathbf{P}:\nabla\mathbf{u}+(m_1+m_2)\mathbf{J}_t\cdot\mathbf{g}\gamma. \tag{4}$$

In Eq. (4), the granular temperature is defined as $T=(n_1T_1+n_2T_2)/n$, where $n=(n_1+n_2)$ is the total number density, $T_i=m_i\langle C_i^2\rangle/3$ is the granular temperature of species i, $C_i=|\mathbf{c}_i-\mathbf{u}_i|$ is the magnitude of the fluctuation velocity of a particle of species i, $\mathbf{c}_i$ is the velocity of a particle of species i, and the brackets $\langle\cdots\rangle$ denote a local volume average. The granular temperature is thus proportional to the average kinetic energy per particle associated with the fluctuations. The first term on the right hand side of Eq. (4) is the energy transferred by diffusion where $\mathbf{J}_t=(n_1\mathbf{v}_1+n_2\mathbf{v}_2)$ is the total diffusion flux on a number basis and $\mathbf{v}_i=(\mathbf{u}_i-\mathbf{u})$ diffusion velocity relative to the mass averaged velocity. The second term corresponds to energy transfer by conduction with conduction flux $\mathbf{q}$, the third term to viscous dissipation, the fourth term to the rate of work done by gravity forces due to a net diffusion flux, and the final term, γ, is the rate of dissipation of energy due to inelastic collisions. Use of Eqs. (2)–(4) requires constitutive equations for the stress, conduction energy flux, energy dissipation due to inelastic collisions and diffusion velocities. Expressions for these for the general case are given in Ref. 23 and we use these results as applied to the two special cases discussed below.

In the first case we consider elastic particles in a gravitational field with no flow ($\mathbf{u}=0$)and with no external forcing at the boundary. In this case, the equilibrium for inelastic particles is clearly $T=0$ (inelastic collapse). However, for elastic particles, the particles assume a uniform granular temperature (determined by the initial condition) at equilibrium, and time-invariant number density profiles for the two species are obtained. This is perhaps the simplest problem involving granular segregation and allows for analysis of pressure-gradient-driven segregation in isolation. The system is isothermal, hence there is no segregation due to temperature gradients. The second case analyzes the equilibrium segregation in steady unidirectional flow of a granular mixture of inelastic particles in a chute. The first problem corresponds to the Monte Carlo simulations and the second to the particle dynamics simulations, both of which are described in Sec. IV.

A. Elastic particles in a gravitational field

Consider a mixture of elastic spherical particles at temperature T in a container and subject to a gravitational field as shown in Fig. 2(a). The container is large enough so that all system boundaries except the lower one have no influence. The system is adiabatic so that at equilibrium, the temperature is uniform and time invariant, and there is no flow in the system. This system, which is conservative and corresponds to the assumptions of the original theory of deHaro *et al.*,[21] is useful primarily for evaluating the theory. The profiles obtained in this case are expected to be similar to those for rapid flows in which the solids volume fractions are relatively low.

The set of governing equations for the system reduces to

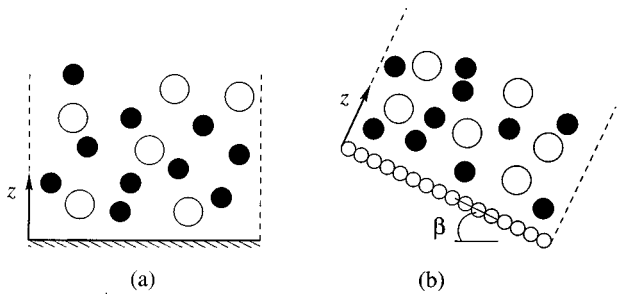

FIG. 2. Schematic view of the systems used for segregation of (a) elastic and (b) inelastic particles. The coordinate system used is indicated. Gravity acts vertically downward.

$$0=-\frac{dp}{dz}-\rho g, \tag{5}$$

where the granular pressure given by

$$p=nT+\frac{2}{3}\pi T\sum_{i=1}^{2}\sum_{k=1}^{2}g_{ik}R_{ik}^3n_in_k, \tag{6}$$

$R_{ik}=(R_i+R_k)$ and $g_{ik}(R_i,R_k,n_i,n_k)$ is the radial distribution function for the pair ik evaluated at the point of contact of the spheres. The radial distribution function for mixtures of hard spheres proposed by Mansoori *et al.*[26] is used here, following Jenkins and Mancini,[23] and is given by

$$g_{ik}=\frac{1}{1-\nu}+\frac{3R_iR_k}{R_i+R_k}\frac{\xi_2}{(1-\nu)^2}+2\left(\frac{R_iR_k}{R_i+R_k}\right)^2\frac{\xi_2^2}{(1-\nu)^2}, \tag{7}$$

where $\xi_p=4\pi(n_1R_1^p+n_2R_2^p)/3$, and $\nu=\xi_3$ is the total volume fraction. All the other equations are identically satisfied since $\mathbf{u}=0$, $\mathbf{v}_1=\mathbf{v}_2=0$(thus $\mathbf{u}_1=\mathbf{u}_2=0$), $T=$constant, and ρ_1 and ρ_2 are time invariant.

The diffusion velocities for the two species reduce to[23]

$$v_{iz}=-\left(\frac{T}{2m_i}\right)^{1/2}nt_{i0}\times\left\{-\frac{\rho_i}{n\rho T}\frac{dp}{dz}+\sum_{k=1}^{2}\frac{n_i}{nT}\left(\frac{\partial\mu_i}{\partial n_k}\right)\frac{dn_k}{dz}\right\},\quad i=1,2, \tag{8}$$

where μ_i is the chemical potential for species i and t_{i0} is a coefficient given in Ref. 24. The chemical potential corresponding to the radial distribution function of Mansoori *et al.*[26] was derived by Reed and Gubbins,[27] and is used in the current analysis. The expression for the chemical potential is

$$\frac{\mu_i}{T}=\ln n_i-\ln(1-\nu)+\frac{4\pi pR_i^3}{3T}+\frac{3\xi_2R_i}{1-\nu}+\frac{3\xi_1R_i^2}{1-\nu}+\frac{9\xi_2^2R_i^2}{2(1-\nu)^2}+3\left(\frac{\xi_2R_i}{\nu}\right)^2\left(\ln(1-\nu)+\frac{\nu}{1-\nu}-\frac{\nu^2}{2(1-\nu)^2}\right)-\left(\frac{\xi_2R_i}{\nu}\right)^3\left(2\ln(1-\nu)+\frac{\nu(2-\nu)}{1-\nu}\right). \tag{9}$$

Setting

$$v_{iz}=0, \quad i=1,2, \tag{10}$$

which must be satisfied at equilibrium, gives four equations together with Eqs. (5) and (6) to obtain the pressure (p) and the number density (n_1, n_2) profiles. Only three of these equations are independent since, by definition, the mass averaged diffusion velocity is zero ($\rho_1 \mathbf{v}_1+\rho_2 \mathbf{v}_2=0$), giving a relation between the two diffusion velocities.

Substituting for the pressure gradient in Eq. (7), and using Eq. (10) we obtain upon simplification

$$m_i g+\left(\frac{\partial \mu_i}{\partial n_1}\right)\frac{dn_1}{dz}+\left(\frac{\partial \mu_i}{\partial n_2}\right)\frac{dn_2}{dz}=0, \quad i=1,2. \tag{11}$$

Eq. (11) together with the appropriate boundary conditions are used to obtain the number density profiles for each of the species. The transport equations are not valid near the flat boundary considered in the problem, and in the Monte Carlo simulations. This is because the transport equations are derived for the bulk of the granular material, and a separate analysis including collisions with the wall is required to obtain the behavior near the boundary (see, e.g., Ref. 28). For comparison to the Monte Carlo and particle dynamics simulations we use the following boundary conditions:

$$n_i=n_{i0} \text{ at } z=z_0, \quad i=1,2, \tag{12}$$

where z_0 is a distance sufficiently far from the lower boundary so that the boundary effect is negligible, and n_{i0} are obtained from the simulations. The complexity of the form of the chemical potential for the general case necessitates numerical solution of the above equations. However, analytical solutions are possible for two special cases and we discuss these below.

1. Ideal gas

In the limit of very low solids volume fractions ($\nu \ll 1$) the mixture behaves as an ideal gas and the chemical potential is obtained from Eq. (9) as

$$\mu_i=T \ln n_i, \quad i=1,2. \tag{13}$$

The governing equations [Eq. (11)] in this case reduce to

$$m_i g+\frac{T}{n_i}\frac{dn_i}{dz}, \quad i=1,2. \tag{14}$$

On integrating Eq. (14) and applying the boundary conditions we get

$$n_i=n_{i0}\exp\left(-\frac{m_i g(z-z_0)}{T}\right), \quad i=1,2. \tag{15}$$

The profile for each component, as might be expected, is independent of the number density of the other component.

The segregation in the system is most clearly apparent when Eq. (15) is cast in terms of the number fraction of component 1, $f=n_1/n$, as

$$\ln\left(\frac{f}{1-f}\right)=\ln\left(\frac{f_0}{1-f_0}\right)-\frac{(m_1-m_2)g(z-z_0)}{T}, \tag{16}$$

where $f_0=n_{10}/n$. If we choose $m_1>m_2$, then Eq. (16) shows that $f/(1-f)=n_1/n_2$ decreases with height. Thus at low volume fractions, the heavier particles migrate to lower levels in the layer, regardless of particle size. In a mixture of equal density particles this implies that the smaller particles rise to the top while the larger particles sink to the bottom. This is the reverse of the effect modeled by Savage and Lun,[4] but is not in conflict with the theory since the sieving-percolation mechanism of their model is not expected to be relevant at the low volume fractions considered here. The effect, however, is in agreement with the results of Nityanand *et al.*[15] for a segregation in a rotating cylinder at high rotational speed. This is discussed in more detail in Sec. VI.

2. Equal sized particles of different density

In this case $R_1=R_2=R$, and the main simplification that arises is in the form of the chemical potential which reduces to

$$\mu_i=T(\ln n_i+F(\nu))+\frac{4\pi p R^3}{3T}, \tag{17}$$

where

$$F(\nu)=\frac{7\nu-3\nu^2-\nu^3}{(1-\nu)^2} \tag{18}$$

and the radial distribution function is $g_{ik}=(2-\nu)/[2(1-\nu)^3]$. Substituting into Eq. (11) we get

$$m_1 g+T\left\{\frac{dn_1}{dz}\left(\frac{1}{n_1}+F'\frac{\partial \nu}{\partial n_1}\right)+\frac{dn_2}{dz}\left(F'\frac{\partial \nu}{\partial n_2}\right)\right\}=0, \tag{19a}$$

$$m_2 g+T\left\{\frac{dn_1}{dz}\left(F'\frac{\partial \nu}{\partial n_1}\right)+\frac{dn_2}{dz}\left(\frac{1}{n_2}+F'\frac{\partial \nu}{\partial n_2}\right)\right\}=0, \tag{19b}$$

where the prime denotes differentiation with respect to ν. Since the radii of the two components are the same we obtain $\partial \nu/\partial n_1=\partial \nu/\partial n_2=4\pi R^3/3$. Subtracting Eq. (19b) from Eq. (19a) we obtain

$$\frac{1}{n_1}\frac{dn_1}{dz}-\frac{1}{n_2}\frac{dn_2}{dz}=-\frac{(m_1-m_2)g}{T}, \tag{20}$$

which upon integration gives

$$\ln\left(\frac{n_1}{n_2}\right)=\ln\left(\frac{n_{10}}{n_{20}}\right)-\frac{(m_1-m_2)g(z-z_0)}{T}. \tag{21}$$

Equation (21) is identical to Eq. (16), so that the number fraction profile [$f(z)$] for equal sized particles of different density is the same as that for an ideal gas, and is independent of the chemical potential. This result is obtained because the local environment experienced by both types of particles (as determined by the pair distribution function, g_{ik}) is the same. Thus the relative motion, which determines the number fraction profile, is independent of the local geometry, and consequently the chemical potential. The number density profile for each component [$n_i(z)$], however, depends on the chemical potential, and must be obtained numerically from Eq. (19).

Casting Eq. (21) in dimensionless form and in terms of the number fraction of component 1, we get

$$\ln\left(\frac{f}{1-f}\right)=\ln\left(\frac{f_0}{1-f_0}\right)-\beta_s(1-\bar{m})(\overline{z-z_0}), \tag{22}$$

where $\beta_s=1/\bar{T}$, $\bar{m}=m_2/m_1$, $\bar{z}=z/R_1$, and the dimensionless temperature is defined as $\bar{T}=T/(m_1gR_1)$. In this case the mass ratio is equal to the density ratio ($\bar{m}=\bar{\rho}$, where $\bar{\rho}=\rho_2/\rho_1$). A similar result was obtained by Khakhar *et al.*[14] using effective medium arguments, with $\beta_s=0.99\bar{T}^{-0.97}$ obtained from Monte Carlo simulations.

B. Inelastic particles in chute flow

Consider the chute flow of inelastic spheres shown schematically in Fig. 2(b). Assuming that the flow is unidirectional, fully developed, and steady, and neglecting any variations in the y direction, the governing equations reduce to

$$0=-\frac{dp}{dz}-\rho g\cos\beta, \tag{23a}$$

$$0=-\frac{d\tau_{zx}}{dz}+\rho g\sin\beta, \tag{23b}$$

$$0=\frac{dq}{dz}-\tau_{zx}\frac{du_x}{dz}-\gamma. \tag{23c}$$

The continuity equation is identically satisfied and the diffusion velocities are given by[23]

$$\nu_{zi}=-\left(\frac{T}{2m_i}\right)^{1/2}\left(nt_{i0}d_{zi}+a_{i0}\frac{d\ln T}{dz}\right)=0,\ i=1,2, \tag{24}$$

with the z component of the diffusion force given by

$$d_{zi}=-\frac{\rho_i}{n\rho T}\frac{dp}{dz}+\frac{n_i}{nT}\sum_{k=1}^{2}\frac{\partial\mu_i}{\partial n_k}\frac{dn_k}{dz}+A_i\frac{d\ln T}{dz}, \tag{25}$$

where a_{i0} and A_i are coefficients given in Eq. (24). The above simplifications result from the assumptions $\mathbf{v}_i=\mathbf{0}$, $u_y=u_z=0$, and assuming that there are no gradients of u_x, p, and T in the x and y directions.

Here we are primarily interested in the segregation problem, and hence do not solve for the velocity and temperature profiles. Instead, we calculate the equilibrium segregation profiles using the temperature profile as an input. In this way, any errors resulting from the calculation of velocity and temperature profiles are not propagated in the calculation of the number density profiles. The temperature profiles are obtained from particle dynamics simulations.

Combining Eqs. (23a), (24), and (25) we obtain

$$nt_{i0}\left(\frac{\rho_i\cos\beta}{n\rho T}+\frac{n_i}{nT}\sum_{k=1}^{2}\frac{\partial\mu_i}{\partial n_k}\frac{dn_k}{dz}\right)+(nt_{i0}A_i+a_{i0})\frac{d\ln T}{dz}=0,\ i=1,2. \tag{26}$$

Upon simplification we get

$$0=m_ig\cos\beta+B_i\frac{dT}{dz}+\left(\frac{\partial\mu_i}{\partial n_1}\right)\frac{dn_1}{dz}+\left(\frac{\partial\mu_i}{\partial n_2}\right)\frac{dn_2}{dz}=0,\ i=1,2, \tag{27}$$

where $B_i=(nA_i/n_i+a_{i0}/(n_it_{i0}))$ and

$$A_i=\frac{n_i}{n}\left(1+\frac{4\pi}{3}n_k(R_i+R_k)^3g_{ik}\frac{m_i}{m_i+m_k}+\frac{16\pi}{3}n_iR_i^3g_{ii}\right),\quad i,k=1,2,\quad i\neq k. \tag{28}$$

Thus, the equations obtained are similar to those derived for elastic particles above, but with an additional flux term due to the temperature gradient. The complexity of the form of B_i does not allow for simple analytical results as derived in Sec. III A for the limiting cases. The expressions for the coefficients a_{i0},t_{i0} given in Ref. 24 are used in our computations.

Computations. The number density profiles are obtained by simultaneously integrating the two governing equations [Eq. (27)]. Simplifying and casting into a dimensionless form we get

$$\frac{d\bar{n}_1}{d\bar{z}}=\frac{\bar{\mu}_{12}\bar{H}_2\bar{\mu}_{22}\bar{H}_1}{\bar{\mu}_{11}\bar{\mu}_{22}\bar{\mu}_{12}\bar{\mu}_{21}}, \tag{29}$$

$$\frac{d\bar{n}_2}{d\bar{z}}=\frac{\bar{\mu}_{21}\bar{H}_1\bar{\mu}_{11}\bar{H}_2}{\bar{\mu}_{11}\bar{\mu}_{22}\bar{\mu}_{12}\bar{\mu}_{21}}, \tag{30}$$

where

$$\bar{\mu}_{ik}=\frac{\partial\bar{\mu}_i}{\partial\bar{n}_k},\quad i,k=1,2 \tag{31}$$

and

$$\bar{H}_i=\bar{m}_i\cos\beta+B_i\frac{d\bar{T}}{d\bar{z}}. \tag{32}$$

The dimensionless initial condition is

$$\bar{n}_i=\bar{n}_{i0},\quad i=1,2\ \text{ at }\ \bar{z}=\bar{z}_0.$$

The overbars denote dimensionless variables; the definition of the dimensionless temperature and distance is the same as given above [following Eq. (22)]. The other dimensionless quantities are defined as : $\bar{n}_i=n_iR_1^3$, $\bar{\mu}_i=\mu_i/m_1gR_1$, $\bar{m}_i=m_i/m_1$, and $\bar{R}_i=R_i/R_1$ for $i=1,2$.

The dimensionless parameters of the system are then the density ratio ($\bar{\rho}$), the size ratio ($\bar{R}$), and the inclination angle of the chute surface (β). In addition, the temperature profile [$\bar{T}(\bar{z})$] and the number densities at position $\bar{z}_0$ ($\bar{n}_{i0}$) are inputs to the problem as formulated here.

The dimensionless equations for elastic particles in an isothermal layer are essentially the same as above but with $\bar{H}_i=\bar{m}_i$. The dimensionless parameters for this system are

the density ratio ($\overline{\rho}$), the size ratio ($\overline{R}$), and the temperature ($\overline{T}$). The number densities at position $\overline{z_0}$ ($\overline{n_{i0}}$) are inputs for the computations.

C. Expressions for diffusion fluxes

While the expressions given in the previous section are convenient to use for computing the number density profiles, they are valid only in the equilibrium state when the diffusion velocities are zero. Expressions of the diffusion fluxes are required for the analysis of the dynamics of simultaneous mixing and segregation. We obtain these from the equations for the diffusion velocities given in Jenkins and Mancini.[23]

The equations in Jenkins and Mancini,[23] as in the previous sections, are written in terms of the number densities (n_1,n_2), the pressure (p), and the temperature (T). However, only three of these variables can be independently specified, hence it is convenient from the point of view of physical clarity to recast these equations in terms of three independent variables: p, T, and f, the number fraction. Diffusion fluxes arise from gradients in each of these variables, and the total diffusion flux is written as the sum of three independent fluxes as is common in standard molecular kinetic theory:[29,30] pressure diffusion (due to gradients in pressure), temperature diffusion (due to temperature gradients, the Soret effect), and ordinary diffusion (due to gradients in number fraction). Since diffusivities scale as the particle diameter squared, temperature and pressure fluxes are significant in granular systems but small in molecular systems. We obtain separate expressions for these fluxes below.

1. Pressure diffusion

Consider first pressure diffusion in isolation, i.e., a system which is isothermal ($\nabla \ln T=0$) and which has no concentration gradients ($\nabla f=0$). The diffusion velocity in this case becomes

$$\mathbf{v}_i=-\left(\frac{T}{2m_i}\right)^{1/2} nt_{i0}\left\{-\frac{\rho_i}{n\rho T}\nabla p + \frac{n_i}{nT}\left(f\frac{\partial \mu_i}{\partial n_1}\nabla n+(1-f)\frac{\partial \mu_i}{\partial n_2}\nabla n\right)\right\} \tag{33}$$

using $n_1=nf$ and $n_2=n(1-f)$. The number density is related to the pressure by the equation of state, and for an isothermal system with uniform number fraction (f) we have

$$\nabla n=\nabla p\left(\frac{\partial n}{\partial p}\right)_{f,T}. \tag{34}$$

Upon substituting in Eq. (33) for ∇n and t_{i0} and simplifying we have

$$\mathbf{v}_i=\frac{D_{ik}nm_k}{\rho^2 T}\left\{m_i-\rho\left(\frac{\partial n}{\partial p}\right)\left(f\frac{\partial \mu_i}{\partial n_1}+(1-f)\frac{\partial \mu_i}{\partial n_2}\right)\right\}\nabla p, \quad i=1,2, \quad k\neq i, \tag{35}$$

where

$$D_{ik}=\frac{3}{8R_{ik}g_{ik}n}\left(\frac{Tm_{ik}}{2\pi m_i m_k}\right)^{1/2} \tag{36}$$

is the binary diffusion coefficient. From Eqs. (35) we get the difference in the diffusion velocities as

$$\mathbf{v}_1-\mathbf{v}_2=-\frac{D_{12}n}{\rho T}\left(\frac{\partial n}{\partial p}\right)\left\{m_2\left(f\frac{\partial \mu_1}{\partial n_1}+(1-f)\frac{\partial \mu_1}{\partial n_2}\right) - m_1\left(f\frac{\partial \mu_2}{\partial n_1}+(1-f)\frac{\partial \mu_2}{\partial n_2}\right)\right\}\nabla p. \tag{37}$$

By definition $\rho_1\mathbf{v}_1+\rho_2\mathbf{v}_2=\mathbf{0}$, hence

$$\mathbf{v}_1=(\mathbf{v}_1-\mathbf{v}_2)\frac{\rho_2}{\rho}. \tag{38}$$

The segregation flux due to a pressure gradient is thus

$$\mathbf{j}_1^p=-\frac{D_{12}\rho_1\rho_2 n}{\rho^2 T}\left(\frac{\partial n}{\partial p}\right)\left\{m_2\left(f\frac{\partial \mu_1}{\partial n_1}+(1-f)\frac{\partial \mu_1}{\partial n_2}\right) - m_1\left(f\frac{\partial \mu_2}{\partial n_1}+(1-f)\frac{\partial \mu_2}{\partial n_2}\right)\right\}\nabla p \tag{39}$$

and $\mathbf{j}_2^p=-\mathbf{j}_1^p$.

2. Temperature diffusion

Consider a system which has only temperature gradients. In this case the diffusion velocity is given by

$$\mathbf{v}_i=-\left(\frac{T}{2m_i}\right)^{1/2} nt_{i0}\left\{\left(A_i+\frac{a_{i0}}{nt_{i0}}\right)\nabla \ln T + \frac{n_i}{nT}\left(f\frac{\partial \mu_i}{\partial n_1}+(1-f)\frac{\partial \mu_i}{\partial n_2}\right)\nabla n\right\}, \quad i=1,2. \tag{40}$$

Upon finding the difference in the diffusion velocities and simplifying as for the case for pressure diffusion above, the diffusion flux due to a temperature gradient is given by

$$\mathbf{j}_1^T=-\frac{D_{12}\rho_1\rho_2 n^2}{\rho^2}\left(\frac{m_2A_1}{n_1}-\frac{m_1A_2}{n_2}\right)\nabla \ln T + \frac{D_{12}\rho_1\rho_2 n}{\rho^2}\left(\frac{m_2a_{10}}{n_1t_{10}}-\frac{m_1a_{20}}{n_2t_{20}}\right)\nabla \ln T \frac{D_{12}\rho_1\rho_2}{\rho^2}\left(\frac{\partial n}{\partial T}\right) \times\left\{m_2\left(f\frac{\partial \mu_1}{\partial n_1}+(1-f)\frac{\partial \mu_1}{\partial n_2}\right) - m_1\left(f\frac{\partial \mu_2}{\partial n_1}+(1-f)\frac{\partial \mu_2}{\partial n_2}\right)\right\}\nabla \ln T \tag{41}$$

and $\mathbf{j}_2^T=-\mathbf{j}_1^T$. The first term in Eq. (41) simplifies to

$$\mathbf{j}_{1,1}^T=\frac{D_{12}\rho_1\rho_2 n}{\rho^2}\nabla \ln T\left\{(m_2-m_1) + \frac{16\pi}{3}\left(m_2n_1g_{11}R_1^3m_1n_2g_{22}R_2^3 + \frac{R_{12}^3g_{12}}{4}\frac{m_1m_2}{m_1+m_2}(n_2-n_1)\right)\right\}. \tag{42}$$

The second term becomes

$$\mathbf{j}_{1,2}^{T}=\frac{D_{12}\rho_1\rho_2 n^2}{\rho^2}K_T(m_2-m_1)\nabla \ln T, \tag{43}$$

where the thermal diffusion ratio is

$$K_T=\frac{4\pi^{1/2}R_{12}^2 g_{12} n_1 n_2}{3n}(M_{21}^{3/2}a_{11}-M_{12}^{3/2}a_{21}). \tag{44}$$

The third term in the equation is very similar to the pressure diffusion flux, and does not simplify further.

3. Ordinary diffusion

The equation for the flux for ordinary diffusion is obtained by considering the diffusion velocity with no pressure and temperature gradients, which reduces to

$$\mathbf{v}_i=-\left(\frac{T}{2m_i}\right)^{1/2} n t_{i0}\left\{\frac{n_i}{nT}\left(n\frac{\partial\mu_i}{\partial n_1}\nabla f+n\frac{\partial\mu_i}{\partial n_2}\nabla(1-f)\right)\right\}. \tag{45}$$

Simplifying Eq. (45) and substituting for the binary diffusivity we get

$$\mathbf{j}_1^f=-\frac{D_{12}m_1m_2n^2}{\rho T}n_1\left(\frac{\partial\mu_1}{\partial n_1}-\frac{\partial\mu_1}{\partial n_2}\right)\nabla f \tag{46}$$

and again $\mathbf{j}_2^f=-\mathbf{j}_1^f$.

4. Discussion

The above equations for the diffusive fluxes are complex, and do not reveal much of the underlying physics. However, some simplifications and insight is possible in two limiting cases which we consider next. For an ideal gas we have

$$\frac{\partial\mu_1}{\partial n_1}=\frac{T}{n_1},\quad \frac{\partial\mu_2}{\partial n_2}=\frac{T}{n_2},\quad \frac{\partial\mu_1}{\partial n_2}=\frac{\partial\mu_2}{\partial n_1}=0,\quad \frac{\partial n}{\partial p}=\frac{1}{T},$$

$$\frac{\partial n}{\partial T}=-\frac{n}{T}$$

so that the pressure diffusion flux reduces to

$$\mathbf{j}_1^p=\frac{D_{12}\rho_1\rho_2}{\rho^2 T}(m_1-m_2)\nabla p, \tag{47}$$

the temperature diffusion flux to

$$\mathbf{j}_1^T=-\frac{D_{12}\rho_1\rho_2 n^2}{\rho^2}K_T(m_1-m_2)\nabla \ln T, \tag{48}$$

and the ordinary diffusion flux to

$$\mathbf{j}_1^f=-\frac{D_{12}m_1m_2n^2}{\rho}\nabla f. \tag{49}$$

Eqs. (47)–(49) correspond to those given in Hirschfelder *et al.*[29] for an ideal gas. The flux equations show that differences in the particle masses result in segregation if a pressure or a temperature gradient exists, however, gradients in concentration result in mixing since the ordinary diffusion flux acts to reduce concentration gradients. Furthermore, if we assume $m_1>m_2$, the equations show that the heavier particles move to regions of higher pressure (due to pressure diffusion) and into regions of lower temperature (due to temperature diffusion). Segregation is independent of the sizes of the particles in this case.

For a mixture of equal sized but different density particles we have

$$\frac{\partial\mu_1}{\partial n_1}=\frac{T}{n_1}+G,\quad \frac{\partial\mu_2}{\partial n_2}=\frac{T}{n_2}+G,\quad \frac{\partial\mu_1}{\partial n_2}=\frac{\partial\mu_2}{\partial n_1}=G,$$

where $G=F'4\pi R^3/3$ [Eq. (18)]. Upon simplification we obtain the pressure flux as

$$\mathbf{j}_1^p=\frac{D_{12}\rho_1\rho_2}{\rho^2 T}(m_1-m_2)\left(\frac{T}{n}+G\right)\frac{\partial n}{\partial p}\nabla p. \tag{50}$$

Further, it can be shown that

$$\left(\frac{T}{n}+G\right)\frac{\partial n}{\partial p}=1, \tag{51}$$

so that

$$\mathbf{j}_1^p=\frac{D_{12}\rho_1\rho_2}{\rho^2 T}(m_1-m_2)\nabla p. \tag{52}$$

Equation (52) is similar in form to that proposed by Khakhar *et al.*[14] based on effective medium arguments. In a similar manner the ordinary diffusion flux simplifies to

$$\mathbf{j}_1^f=-\frac{D_{12}m_1m_2n^2}{\rho}\nabla f. \tag{53}$$

Eqs. (52) and (53) for the pressure and ordinary diffusion fluxes are identical to the corresponding equations for an ideal gas; the form of the binary diffusivity, however, is different. The temperature diffusion flux does not simplify to a significant extent in this case.

IV. COMPUTATIONS:

A. Monte Carlo simulations

Monte Carlo simulations are used here to obtain the equilibrium number fraction profiles for a mixture of elastic hard spheres in a gravitational field as shown in Fig. 2(a). The system is isothermal. Starting from an initially random configuration the system is driven to equilibrium by means of perturbations which on average either reduce or keep unchanged (at equilibrium) the potential energy of the system. The procedure used is briefly described below.

Particles, randomly distributed in the domain initially, are sequentially given random displacements. A displacement is accepted with probability $\min(1,P_{\text{ran}})$ if it does not result in overlap with other particles, where

$$P_{\text{ran}}=\exp\left(-\frac{m_i g\Delta z}{T}\right),\quad i=1 \text{ or } 2 \tag{54}$$

and Δz is the upward vertical component of the displacement. Positions of pairs of particles are also interchanged at random and the interchange is accepted with probability $\min(1,P_{\text{int}})$ if there is no overlap of particles, where

$$P_{\text{int}}=\exp\left(-\frac{(z_i-z_k)(m_i-m_k)g}{T}\right) \tag{55}$$

and i and k denoted the indices of the particles being interchanged. In physical terms, the above formulation results in acceptance of all moves which produce a decrease of the potential energy of the system, whereas moves which produce an increase in the potential energy are accepted with a probability which depends on the granular temperature according to Eqs. (54)–(55) given above. The interchange moves are used since they result in a faster convergence to equilibrium when particle sizes are nearly equal and when the solids volume fractions are low.

Using the dimensionless variables defined in Sec. III, the equations for the probability reduce to

$$P_{\text{ran}} = \exp\left(-\frac{\bar{m}_i \Delta \bar{z}}{\bar{T}} \right), \quad i = 1 \text{ or } 2, \tag{56a}$$

$$P_{\text{int}} = \exp\left(-\frac{(\bar{z}_i - \bar{z}_k)(\bar{m}_i - \bar{m}_k)}{\bar{T}} \right), \tag{56b}$$

where $\bar{m}_1 = 1$ and $\bar{m}_2 = \bar{m}$.

Simulations are carried out using 600 particles in a domain with a square cross section (25 particle diameters wide) and the height of the domain is taken to be large enough so that the particles are always far from the upper surface. The upper and lower surfaces are taken to be reflecting and periodic boundary conditions are applied at the side boundaries.

B. Particle dynamics

Particle dynamics simulations are analogous to molecular dynamics simulations for the study of gases and liquids. The trajectories of particles in a flowing granular medium are obtained from the equations for the conservation of linear and angular momentum, or explicit integration of out-of-balance forces on the particles. Forces taken into account in particle dynamics include the forces due to gravity, interparticle collisions (or contacts). We simulate chute flow of a mixture of spherical particles for two cases: inelastic frictionless particles and inelastic frictional particles. The computational procedures used are briefly given below.

1. Inelastic frictionless particles

In this case the particles do not experience torque and hence do not rotate. This results in simplification of the analysis since the conservation of angular momentum equation is satisfied, and the trajectories can be calculated from the conservation of linear momentum alone. Collisions between particles are assumed to be instantaneous and each collision results in a fractional decrease in the relative velocity $(1-e)$, where e is the restitution coefficient, in the component along the line joining the centers of the colliding spheres at contact. The components normal to this direction are conserved. In the computations the time for the first collision is determined and all particles moved for this time interval. The velocities of the colliding pair of particles are updated, the time for the next collision determined, and the procedure is repeated. Starting with a random configuration of particles, the flow is continued until steady state velocity and composition profiles are obtained.

A total of 600 particles are used in a domain of square cross section (15 particle diameters wide) and the lower surface of the domain comprises a layer of fixed beads inclined at an angle β [Fig. 2(b)]. The upper surface of the domain is taken to be high enough so as not to be far from the particles, and periodic boundary conditions are used on the side boundaries. The radius of the particle forming the lower surface is taken to be $0.5R_1$ and the coefficient of restitution to be $e = 0.9$.

2. Inelastic frictional particles

Several force models for particle–particle interactions have been proposed previously, and a review is given in Refs. 8 and 31. In the present work the normal force is chosen to be

$$F_n = k_1 \alpha \tag{57a}$$

for loading, and

$$F_n = \begin{cases} k_2(\alpha - \alpha_0) & \text{for } \alpha > \alpha_0 \\ 0 & \text{for } \alpha \leqslant \alpha_0 \end{cases} \tag{57b}$$

for unloading. The deformation is assumed to be proportional to the overlap between particles $\alpha = (R_i + R_j - D_{ij})$ where D_{ij} is the distance between the centers of the colliding spheres, and α_0 is the permanent deformation. The above model simulates an elastic-plastic solid with a velocity independent coefficient of restitution $e = \sqrt{k_1/k_2}$. The tangential force between particles in contact is taken to be

$$F_t = \begin{cases} k_t s & \text{for } k_t s \leqslant \mu F_n \\ \mu F_n & \text{for } k_t s \leqslant \mu F' \end{cases} \tag{58}$$

where s is the relative displacement of the surfaces in contact, and μ is the coefficient of static friction. The model is a simplified version of that proposed by Mindlin.[32]

The boundary conditions used are the same as for the inelastic frictionless particles given above. For all simulations, the cross section of the domain is 10 (large) particles wide and 14 particles long and the (dimensionless) parameters used in the model are: $k_1 = 1 \times 10^4$, $e = 0.7$, $k_t = 0.8k_1$, and $\mu = 0.5$. For the density simulations, 1000 particles are used, resulting in a flowing layer about 9 particles deep—the total number of particles increases for the size segregation case as the size ratio decreases. The boundary particles are the same size as the bulk particles for the case of density segregation and are one-quarter of the size of the large particles for the case of size segregation, so that the perceived ''roughness'' is approximately the same for all size ratios.

V. RESULTS AND DISCUSSION

We present results below for two types of systems: (i) equal sized particles with different density and (ii) equal density particles but with different sizes. In both cases the role of pressure and temperature diffusion are discussed. All the results presented below are in terms of the dimensionless variables; the overbars are omitted for convenience.

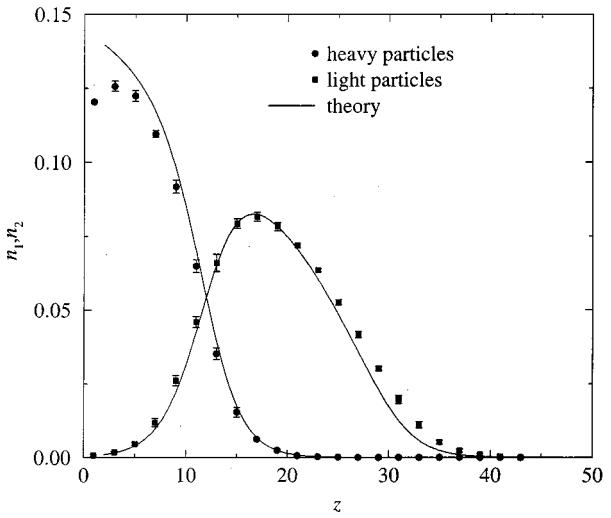

FIG. 3. Equilibrium dimensionless number density profiles for equal sized elastic particles with different density under isothermal conditions. The dimensionless granular temperature is $T=1$, and the density ratio is $\rho=0.5$. Points are results of Monte Carlo simulations and the error bars show the standard deviation; solid lines are predictions of the kinetic theory.

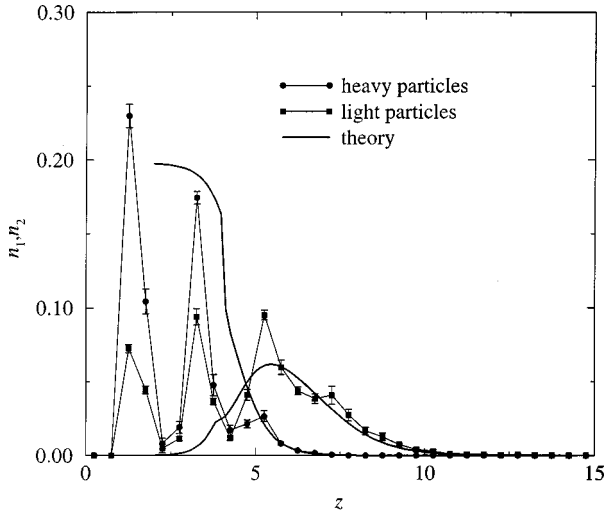

FIG. 5. Equilibrium dimensionless number density profiles for equal sized inelastic, frictionless particles with different density in chute flow. The density ratio is $\rho=0.5$ and the inclination of the chute is $\beta=25°$. Points are results of particle dynamics simulations and the error bars show the standard deviation; thick solid lines are predictions of the kinetic theory using the temperature profile shown in Fig. 6.

A. Equal sized particles with different density

Figure 3 shows the number fraction profiles for elastic particles in a gravitational field obtained from Monte Carlo simulations. The higher density particles are concentrated at lower levels in the layer. This segregation results entirely from pressure diffusion, since the temperature is constant. The predicted number density profiles obtained from Eq. (11) are also shown. There is very good agreement between theory and computations even at high volume fractions. Figure 4 shows the variation of $\ln(n_1/n_2)$ with dimensionless height (z) together with predictions of the theory. Straight lines with slope $M=-(1-\rho)/T$ are obtained in accordance with theory. This is valid even at high volume fractions where there are deviations from theory for the computed volume fraction profiles. The cause for the deviation between theory and experiment at the bottom of the layer is most likely due to the boundary effects. There are no adjustable parameters in the theory.

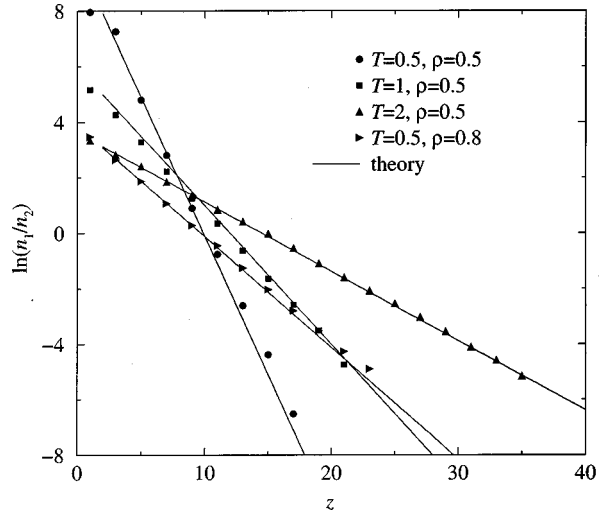

FIG. 4. Equilibrium number ratio profiles for equal sized elastic particles with different density under isothermal conditions. Results for different density ratios and temperatures are shown. Points are results of Monte Carlo simulations and solid lines are predictions of the kinetic theory.

Chute flow of inelastic frictionless particles results in number fraction profiles which are qualitatively different from those obtained above (Fig. 5). Since the particles are of equal size, they arrange themselves into layers near the lower surface as is apparent from the large fluctuations in the number density. As in the previous case, the denser particles sink to the lower portions of the flowing layer, however, complete exclusion of the lighter particles from the lowest layers does not occur, as above. Prediction of the number density profiles, by integration of Eq. (27), requires the temperature profile in this case. The dimensionless temperature variation with height is given in Fig. 6, and is nearly linear for the case considered. A second-order polynomial is fitted to the data and is used to calculate the temperature gradient and temperature at any position for the integration. A comparison of theory and predictions are shown in Fig. 5. The predictions are reasonably good away from the boundary region, however, there are significant deviations close to the boundary. Boundary effects are large in this case most likely due to the layering of the particles. Another source of error is the kinetic theory estimation of the coefficients a_{i0}, t_{i0}, and A_i, which determine the temperature diffusion flux; the validity of these expressions remains to be checked. Variation of the number ratio with height is shown in Fig. 7. Again agreement between theory and computations in the region away from the boundary is very good. There are no adjustable parameters in the theory.

Consider next the relative importance of the temperature gradient and the pressure gradient on the equilibrium profile. Figure 8 shows a comparison of the profiles obtained using the full theory, profiles obtained omitting the terms containing the temperature gradient from Eq. (27), and profiles ob-

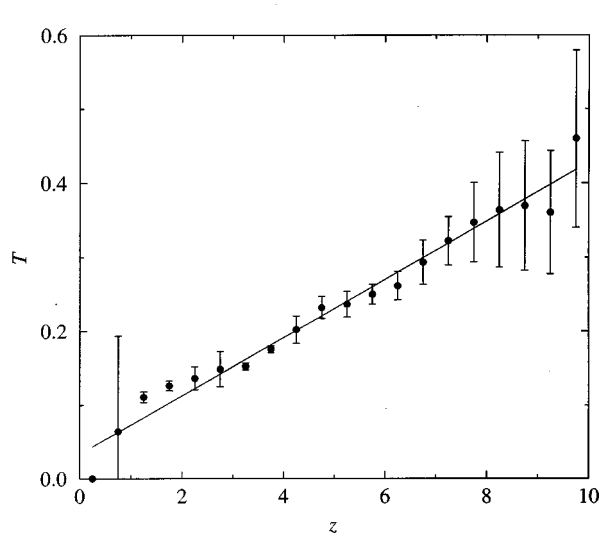

FIG. 6. Temperature profile obtained from particle dynamics simulations for equal sized inelastic, frictionless particles with different density in chute flow. The density ratio is $\rho=0.5$ and the inclination of the chute is $\beta=25°$. Points are results of particle dynamics simulations and the error bars show the standard deviation; the solid line is a second-order polynomial fitted to the data.

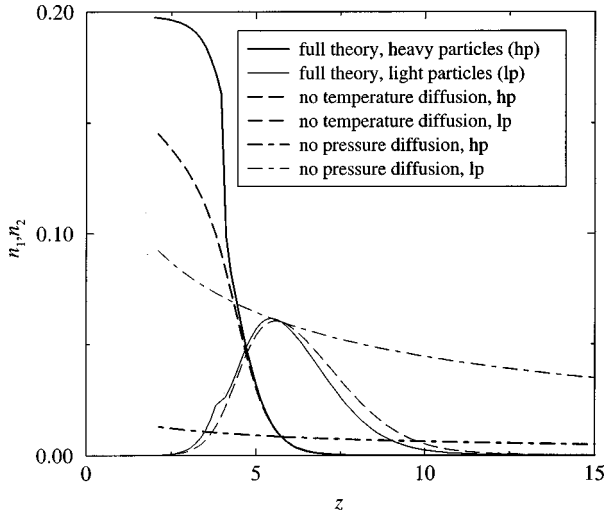

FIG. 8. Theoretically predicted number density profiles for inelastic frictionless particles in chute flow for the conditions indicated in the legend. The density ratio is $\rho=0.5$, the inclination of the chute is $\beta=25°$, and the temperature profile shown in Fig. 6 is used.

tained omitting the terms containing the temperature gradient from Eq. (27). The profiles for the full theory and those without temperature diffusion are very similar, indicating that temperature diffusion does not play an important role in the process. The number ratio profile without temperature diffusion for one density ratio is also plotted in Fig. 7 and it coincides with the curve obtained from the full theory. Thus for equal sized particles, temperature diffusion has no effect on the segregation. This is most clearly brought out by computations including temperature diffusion but omitting pressure diffusion. The number density of each component varies with height in this case (Fig. 6), however, there is no segregation since the number ratio is independent of height (Fig. 7). The number ratio profile omitting the temperature gradient term is curved (Fig. 7), as compared to the straight lines obtained for the isothermal system (Fig. 4), because the variation of the pressure diffusion due to the varying temperature is taken into account.

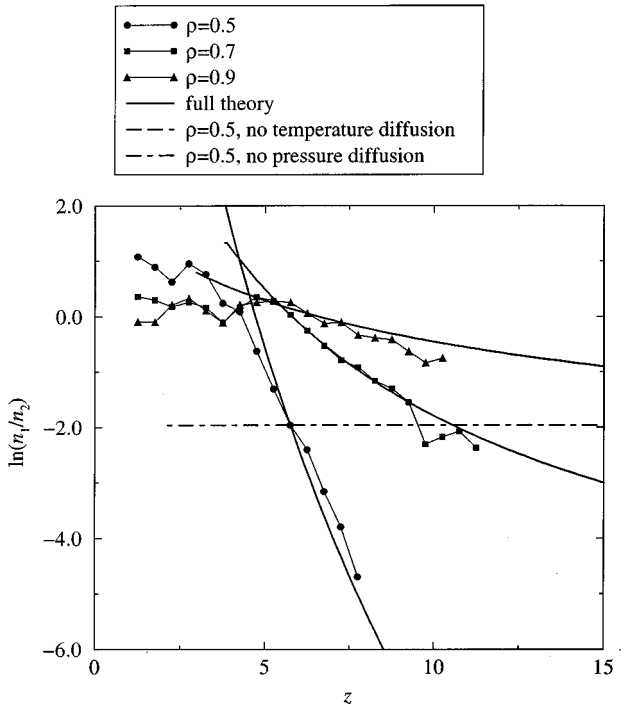

FIG. 7. Equilibrium dimensionless number ratio profiles for equal sized inelastic, frictionless particles with different density in chute flow. The inclination of the chute is $\beta=25°$ and different density ratios are used. Points are results of particle dynamics simulations and the thick lines are predictions of the kinetic theory for the conditions indicated in the legend. The line for the case of no temperature diffusion coincides with that for the full theory for $\rho=0.5$.

Typical number density profiles obtained from particle dynamics simulations for inelastic, frictional particles of equal size but different density are shown in Fig. 9. As in the previous cases, the denser particles sink to the bottom of the layer, and nearly complete segregation is achieved. The extent of segregation is apparent from the number ratio profiles which are shown for three different density ratios in Fig. 10. Straight lines are obtained in all three cases, in apparent agreement with theory. Predictions of the theory in this case give straight lines, however, the slopes of the theoretically predicted lines are more than an order of magnitude larger than those obtained from particle dynamics. The high slopes result from the very low granular temperatures in the flow (Fig. 11). Recall that the slope is inversely proportional to the temperature $[M=-(1-\rho)/T]$. In hindsight, it is not surprising that the theory does not work for this case. Dissipation is large in this system, and this causes the system to deviate significantly from the assumption built into the theory—that the system is nearly conservative. Dissipation directly affects the temperature, and one possible way of comparing the theory to the computations is to find some *effective* temperature for the flow. This was done by fitting straight lines to the computational data in Fig. 10, and cal-

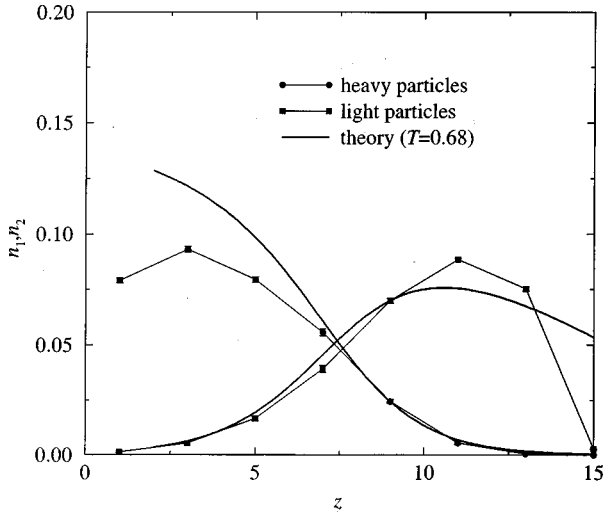

FIG. 9. Equilibrium dimensionless number density profiles for equal sized inelastic, frictional particles with different density in chute flow. The density ratio is $\rho = 0.5$ and the inclination of the chute is $\beta = 24°$. Points are results of particle dynamics simulations and the error bars show the standard deviation; thick solid lines are predictions of the kinetic theory using an effective temperature obtained from the slope of the line in Fig. 10.

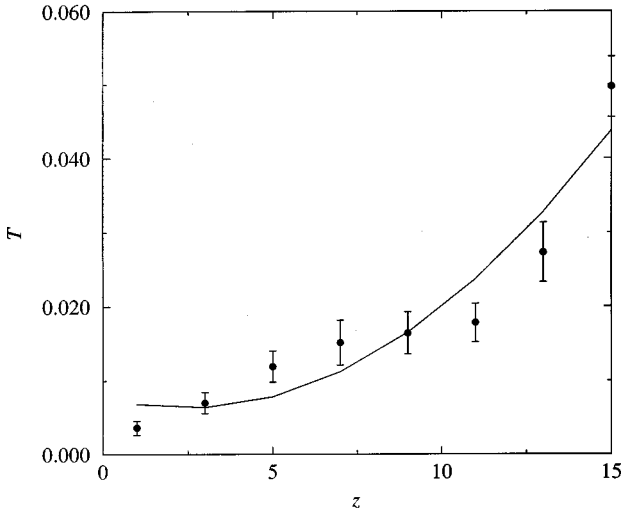

FIG. 11. Computed temperature profile for equal sized inelastic, frictional particles with different density in chute flow. The density ratio is $\rho = 0.5$ and the inclination of the chute is $\beta = 24°$. Points are results of particle dynamics simulations and the error bars show the standard deviation; the solid line is a second-order polynomial fitted to the data.

culating the corresponding temperature from the expression for the slope (M) given above. Computed number density profiles using this constant effective temperature are in reasonable agreement with particle dynamics results (Fig. 9). This indicates that the functional form for the pressure flux obtained from theory is valid even for the case of highly dissipative systems, however, the magnitude of the flux must be estimated empirically.

B. Equal density particles with different sizes

Figures 12 and 13 show the results of Monte Carlo simulations for elastic particles with equal density but different sizes. The system is isothermal hence segregation is only due to pressure diffusion. The number density profiles (Fig. 12) show that the smaller particles by and large concentrate in the upper region of the layer. The number ratio profiles also decrease monotonically with distance over most of the layer indicating that pressure diffusion flux of the larger particles is in the downward direction. In regions of higher volume fraction (Fig. 14), however, there is a reversal of this trend, implying also a reversal in the direction of the pressure diffusion flux. Though the magnitude of the effect is small it indicates that different mechanisms are operative in the two regions. In the low volume fraction region the pressure diffusion flux direction is independent of the particle size and the heavier (in this case larger) particles sink into the regions of higher pressure [Eq. (52)] as found above. In the higher

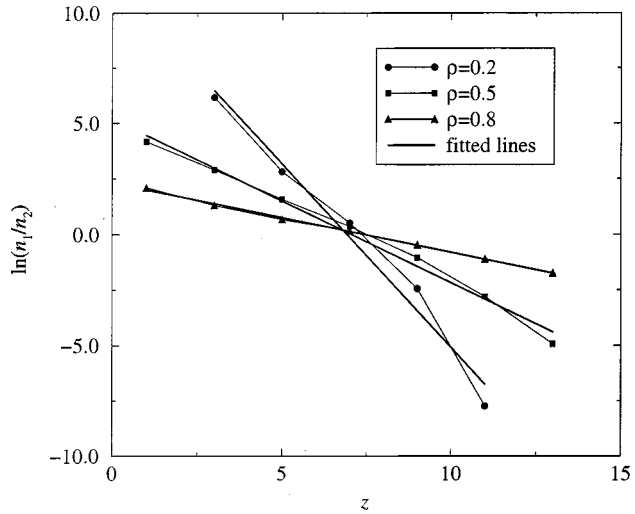

FIG. 10. Equilibrium dimensionless number ratio profiles for equal sized inelastic, frictional particles with different density in chute flow. The inclination of the chute is $\beta = 24°$ and different density ratios are used. Points are results of particle dynamics simulations and the thick lines are least squares to the data.

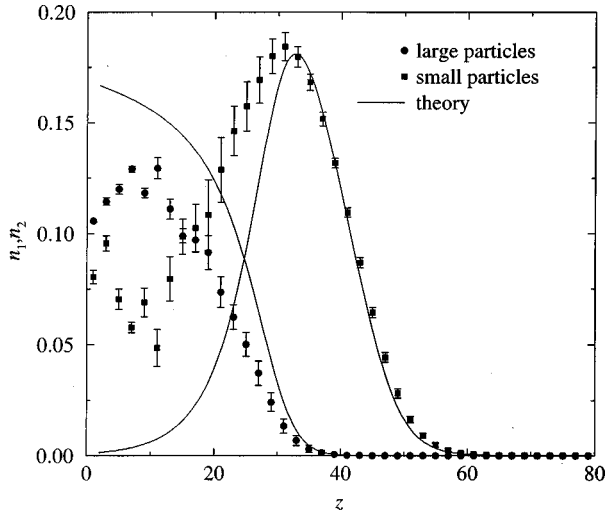

FIG. 12. Equilibrium dimensionless number density profiles for equal density elastic particles with different sizes under isothermal conditions. The dimensionless granular temperature is $T = 1$, and the size ratio is $R = 0.7$. Points are results of Monte Carlo simulations and the error bars show the standard deviation; solid lines are predictions of the kinetic theory.

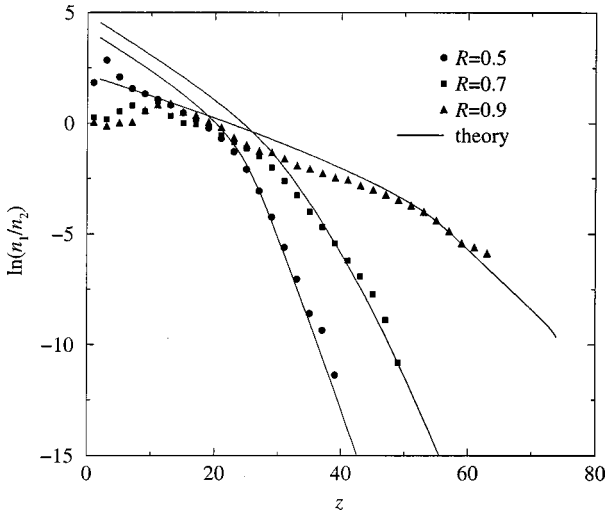

FIG. 13. Equilibrium number ratio profiles for equal density elastic particles with different sizes under isothermal conditions. Results for different size ratios and temperature $T=1$ are shown. Points are results of Monte Carlo simulations and solid lines are predictions of the kinetic theory.

volume fraction region gaps between particles are small, thus percolation of the smaller particles becomes predominant, so that the flux of the larger particles is upward and thus into the lower pressure region.

Predictions of the theory are in very good agreement with computed results in the low volume fraction regions ($\nu<0.2$). At higher concentrations there are deviations, and a qualitative difference is that the theory does not show a reversal of the pressure diffusion flux. This is due to the inadequacy of the expression for the chemical potential at the high volume fractions near the bottom of the layer; there is no temperature diffusion flux in this case. Consider next the conditions for the flux reversal to occur.

Expressing the chemical potential as $\mu_i=\mu_i^0+\mu_i^E$, where μ_i^0 is the ideal gas chemical potential and μ_i^E is the excess chemical potential, and assuming for simplicity an

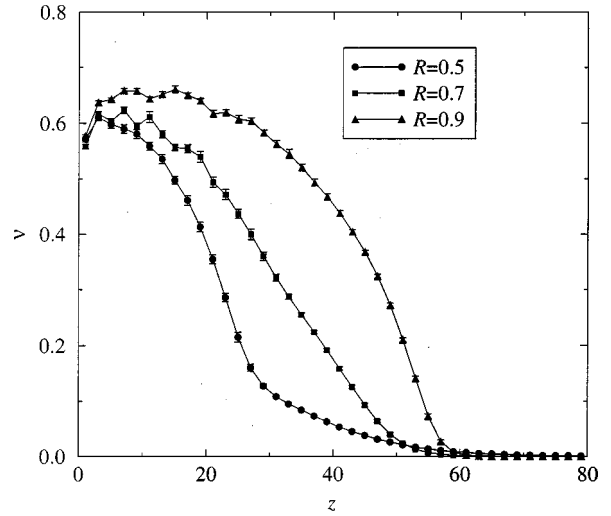

FIG. 14. Equilibrium volume fraction profiles for equal density elastic particles with different sizes under isothermal conditions obtained from Monte Carlo simulations. Results for different size ratios and temperature $T=1$ are shown.

infinitesimally small number density of the smaller particles ($n_2\approx 0$), the pressure diffusion flux reduces to

$$\mathbf{j}_1^p=\frac{D_{12}\rho_1\rho_2}{\rho^2}\left(\frac{\partial n}{\partial p}\right)\times\left\{m_1m_2+\frac{m_1n_1}{T}\frac{\partial\mu_2^E}{\partial n_1}-\frac{m_2n_1}{T}\frac{\partial\mu_1^E}{\partial n_1}\right\}\nabla p. \quad (59)$$

For low volume fractions, $\mu_i^E=0$ so that the term in the brackets $\{\cdots\}$ is positive ($m_1>m_2$ since subscript ''1'' refers to the larger particles). The term must change sign to effect flux reversal. The following alternate definition of the excess chemical potential allows physical interpretation of Eq. (59) in the context of flux reversal[33]

$$\mu_i^E=-T\ln P_i^{\mathrm{ins}}. \quad (60)$$

Here, P_i^{ins} is the probability of insertion of particle i at a randomly chosen position in the granular mixture. For very low solids volume fractions $P_i^{\mathrm{ins}}=1$ so that the excess chemical potential vanishes as required. For high volume fractions the probability of inserting a large particle is much smaller than that for inserting a small particle, thus in this limit we have $\mu_1^E\gg\mu_2^E$. The condition for flux reversal in terms of the insertion probability is

$$-\frac{\partial}{\partial\ln n_1}(R^3\ln P_1^{\mathrm{ins}}-\ln P_2^{\mathrm{ins}})>(1-R^3), \quad (61)$$

where $R^3=m_2/m_1$ since the densities are equal. The condition given by Eq. (61) shows that it is not the difference in the insertion probabilities but how these probabilities vary with number density that determines the direction of the pressure flux. Further the condition is independent of temperature. For small size ratios ($R\ll 1$), the change in the insertion probability of the smaller particles with change in the number density of the larger particles would be small at infinite dilutions as considered here. The criterion for flux reversal thus becomes

$$-\frac{\partial\ln P_1^{\mathrm{ins}}}{\partial\ln n_1}>\frac{1}{R^3}. \quad (62)$$

Since $-\ln P_1^E\to\infty$ as the limit of close packing is approached, it is likely that the above criterion will be satisfied. Thus at high volume fractions percolation of the smaller particles should occur due to pressure diffusion alone.

The above discussion shows that the percolation mechanism proposed by Savage and Lun[4] is described by the kinetic theory. The relation between the flux and the insertion probability in the two theories are, however, different. The mechanism of size segregation depends on the local solids volume fraction—percolation of the smaller particles dominates at high volume fractions whereas the smaller particles rise to the top at low volume fractions.

Figure 15 shows the number density profiles for slightly inelastic, equal density frictionless particles with different sizes. As in the case of elastic particles discussed above, the small particles by and large concentrate in the upper regions of the layer, and again there is evidence of flux reversal in the lower high volume fraction region. This is also evident in the number ratio profiles shown in Fig. 16. Theoretical pre-

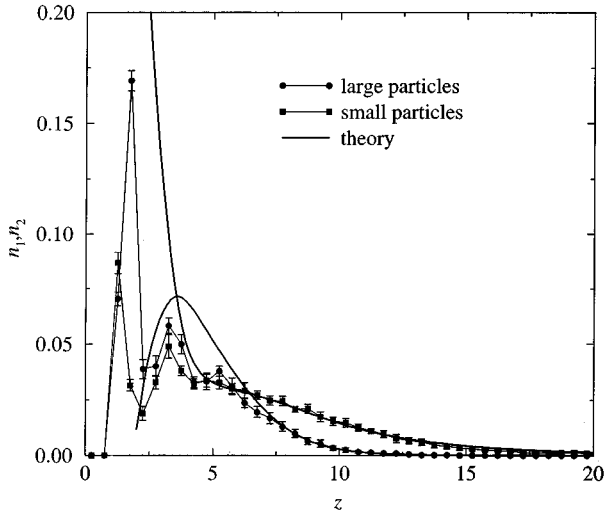

FIG. 15. Equilibrium dimensionless number density profiles for equal density inelastic, frictionless particles with different sizes in chute flow. The size ratio is $R=0.7$ and the inclination of the chute is $\beta=25°$. Points are results of particle dynamics simulations and the error bars show the standard deviation; thick solid lines are predictions of the kinetic theory using the temperature profile shown in Fig. 17.

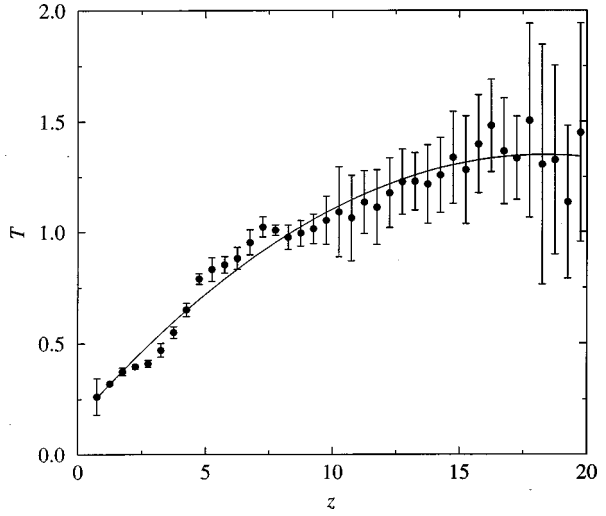

FIG. 17. Computed temperature profile for equal sized inelastic, frictionless particles with different density in chute flow. The size ratio is $R=0.7$ and the inclination of the chute is $\beta=25°$. Points are results of particle dynamics simulations and the error bars show the standard deviation; the solid line is a second-order polynomial fitted to the data.

dictions of the number density profiles and the number ratio profiles, using the temperature profile obtained from the particle dynamics simulations as an input (Fig. 17), are in good agreement with computed results in the low volume fraction regions (Figs. 15 and 16). There are significant differences between theory and computations in the high volume fraction region, and these are due to both boundary effects (which cause particle layering) and deficiency of the expression for the chemical potential used at high volume fractions. Notice that the theory predicts flux reversal and significant segregation in the high volume fraction region—the number ratio sharply increases with distance in this region (Fig. 16).

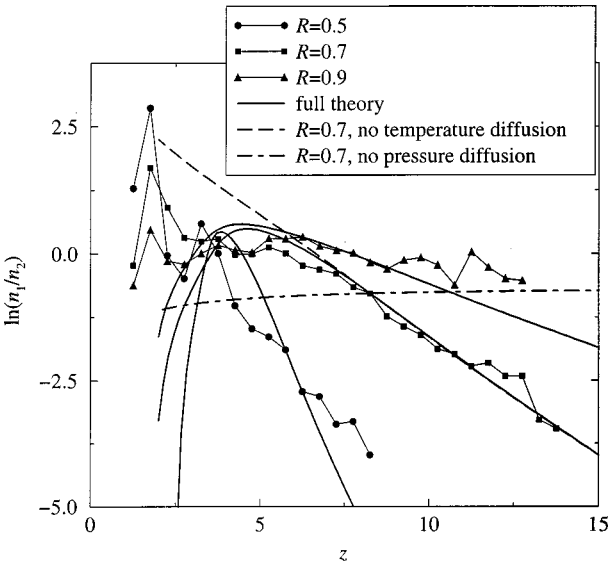

FIG. 16. Equilibrium dimensionless number ratio profiles for equal density inelastic, frictionless particles with different sizes in chute flow. The inclination of the chute is $\beta=25°$and different size ratios are used. Points are results of particle dynamics simulations and the thick lines are predictions of the kinetic theory for the conditions indicated in the legend.

Thus the existence of a small positive temperature gradient along with a pressure gradient in a high volume fraction region results in strong reverse segregation, with the smaller particles concentrating in the lower levels.

The relative importance of the temperature and pressure effects are examined using the theory in Fig. 18. The effect of excluding the temperature gradient terms is greatest in the high-volume fraction regions. As in the case of elastic particles, no flux reversal is seen without temperature diffusion and the number ratio profile is monotonic (Fig. 16). Excluding the pressure diffusion results in segregation of the smaller particles in the lower regions of the bed, though the extent of segregation is not large. This is in contrast to the equal sized particles of different density which did not result in any segregation.

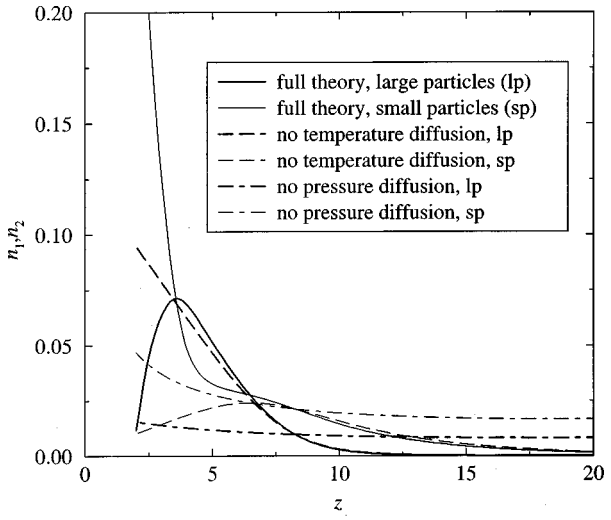

FIG. 18. Theoretically predicted number density profiles for inelastic frictionless particles in chute flow for the conditions indicated in the legend obtained from the kinetic theory. The density ratio is $R=0.7$, the inclination of the chute is $\beta=25°$, and the temperature profile shown in Fig. 17 is used.

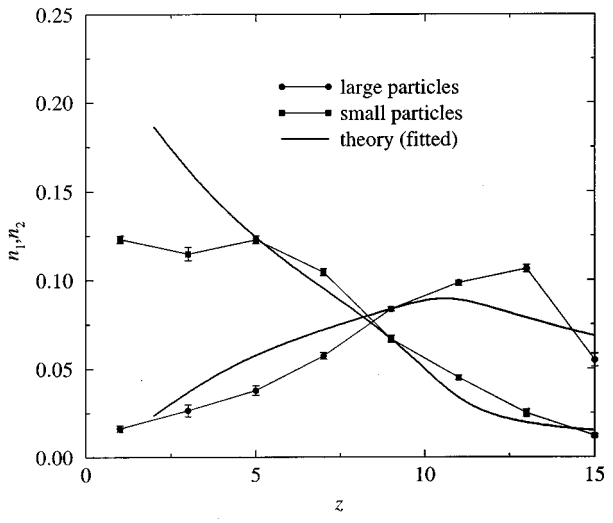

FIG. 19. Equilibrium dimensionless number density profiles for equal density inelastic, frictional particles with different sizes in chute flow. The size ratio is $R=0.9$ and the inclination of the chute is $\beta=24°$. Points are results of particle dynamics simulations and the error bars show the standard deviation; thick solid lines are predictions of the kinetic theory using an effective linear temperature profile obtained by fitting the theory to the data in Fig. 20.

Finally, the typical equilibrium segregation profiles for inelastic, frictional particles is shown in Fig. 19 and number ratio profiles for three different size ratios are shown in Fig. 20. In contrast to the cases of elastic particles and slightly inelastic particles considered above, here the smaller particles concentrate in the lower part of the layer (Fig. 19) and the number ratio of the larger particles increases monotonically with height (Fig. 20). This implies that the segregation flux of the larger particles is upward throughout the layer, as compared to the other two cases where it is downward in the low volume fraction regions and reverses direction in the high volume fraction region. This behavior is most likely obtained because the volume fraction of solids is uniformly high across the layer (Fig. 21).

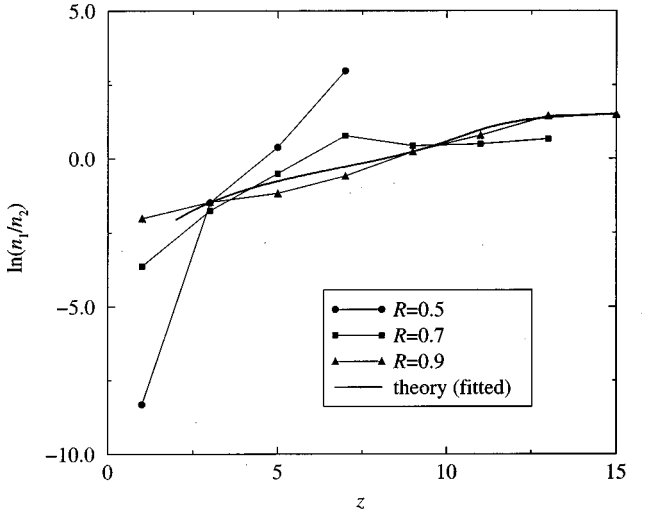

FIG. 20. Equilibrium dimensionless number ratio profiles for equal density inelastic, frictional particles with different sizes in chute flow. The inclinations of the chute are $\beta=24°$ for $R=0.5,0.9$ and $\beta=26°$ for $R=0.7$. Points are results of particle dynamics simulations and the thick line is a fit to the data for $R=0.9$ using a linear effective temperature profile.

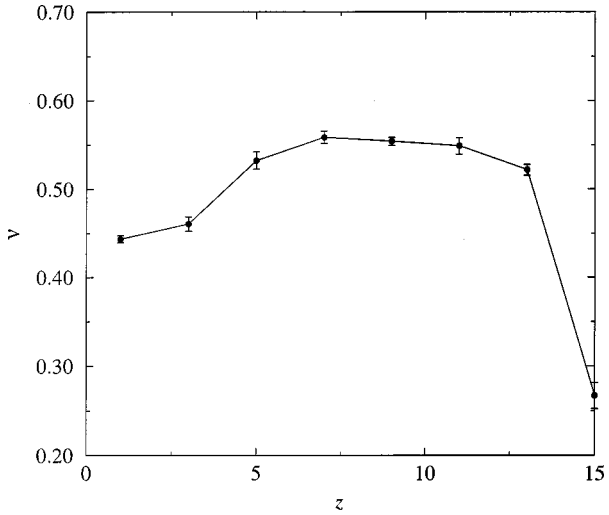

FIG. 21. Equilibrium volume fraction profiles for equal density inelastic, frictional particles in chute flow obtained from particle dynamics simulations for $\beta=24°$ and $R=0.9$.

As in the case of equal sized, inelastic, frictional particles with density differences discussed in Sec. V A, using the computed temperature profile as an input to the calculation of the number density profile does not give reasonable predictions. The theoretical predictions shown in Figs. 19 and 20 are obtained by choosing a linear temperature profile (with the temperature increasing with height) so that the number ratio profile is well-described (Fig. 20). The predictions of the number density profiles are then reasonable (Fig. 19).

VI. CONCLUSIONS

Computational and theoretical analyses of size and density segregation in a chute flow of spherical particles are presented. The effects of particle inelasticity and interparticle friction are considered by means of the computations. Theoretical predictions of the equilibrium number density profiles are obtained from the kinetic theory of hard sphere mixtures (de Haro *et al.*[21]) which is valid for slightly inelastic particles.

Computational results for density segregation are qualitatively similar for all three types of particles considered (elastic, slightly inelastic, and inelastic and frictional) in that the denser particles sink to lower regions, and the variation of number ratio profile with height is nearly linear. In the absence of temperature diffusion, a simple expression for the pressure diffusion flux is obtained, and an analytical result for the number ratio profile is obtained. These are in agreement with earlier results obtained using a different approach. Predictions of the theory are in excellent agreement with computational results for the elastic particles (even at high volume fractions), and in good agreement for the case of slightly inelastic particles away from the region where layering of the particles occurs. In the case of inelastic frictional particles, the computed temperatures are low, and using

these in the theory gives poor predictions. However, reasonable predictions of the number density profiles are obtained if the temperature obtained by fitting the theory to the number ratio profile is used. Temperature diffusion has little effect on the segregation for equal sized particles. The computations indicate that Eq. (52) describes density segregation well, if the temperature is treated as an empirical parameter of the problem for the case of inelastic frictional particles.

The case of size segregation is more complex. Elastic and slightly inelastic particles show concentration of the smaller particles in the upper regions of the layer, indicating a net downward flux of the larger particles. In the lower regions where the volume fraction is higher there is a reversal of the flux. However, qualitatively different behavior is observed in the case of inelastic, frictional particles, with the smaller particles concentrating in the lower regions of the layer, which implies that the net flux of the larger particles is upward throughout the layer. Comparisons of theory to the results for elastic particles shows very good agreement for solid volume fractions $\nu < 0.2$. However, at higher solid volume fractions there are deviations between the two, and the theory does not predict flux reversal. Improved predictions may be possible with a more accurate expression for the chemical potential. Theoretical predictions are reasonably good for inelastic particles in the low volume fraction regions; the theory predicts a strong flux reversal in the high volume fraction regions as a result of a temperature gradient (temperature increasing with height). Reasonable predictions of the number density profiles for inelastic, frictional particles are obtained if an effective temperature profile is used.

The computational and theoretical results presented here go some way toward explaining the experimental results of Nityanand *et al.*[15] for radial segregation discussed earlier (Sec. II). At low rotational speeds, slow flow in the cascading layer of the rotating drum results in high solids volume fractions, and thus smaller particles would sink to lower parts of the layer, resulting in the formation of a core of the smaller particles. However, at higher speeds because of the lower volume fractions the flux of the smaller particles changes direction, resulting in the formation of a core of the larger particles with the smaller particles at the periphery.

The computational results presented show the utility of the kinetic theory expressions for the analysis of segregation in more complex systems. The theory appears to be quite good for mixtures of nearly elastic, equal sized particles at all volume fractions, and for mixtures of nearly elastic, different sized particles at low volume fractions. A more accurate constitutive equation for the chemical potential is needed for mixtures of nearly elastic, different sized particles at higher volume fractions. The above conclusions hold for mixtures of inelastic and frictional particles provided an effective temperature is used. A fundamental understanding of the effective temperature for highly dissipative systems would render the theory more useful for application.

ACKNOWLEDGMENTS

Financial support from NSF (Fluids and Particulate Systems), DOE (Division of Basic Energy Sciences), and The Petroleum Research Fund, administered by the American Chemical Society, is gratefully acknowledged. D.V.K. acknowledges the financial support of the Department of Science and Technology, India, through the award of the Swarnajayanti Fellowship (DST/SF/8/98).

[1] J. C. Williams, ''The segregation of particulate materials,'' Powder Technol. **15**, 245–256 (1976).
[2] M. B. Donald and B. Roseman, ''Mixing and de-mixing of solid particles: Part I. Mechanisms in a horizontal drum mixer,'' Br. Chem. Eng. **7**, 749–752 (1962).
[3] J. Bridgwater, ''Fundamental powder mixing mechanisms,'' Powder Technol. **15**, 215–231 (1976).
[4] S. B. Savage and C. K. K. Lun, ''Particle size segregation in inclined chute flow of cohesionless granular solids,'' J. Fluid Mech. **189**, 311–335 (1988).
[5] S. S. Hsiau and M. L. Hunt, ''Granular thermal diffusion in flows of binary-sized mixtures,'' Acta Mech. **114**, 121–137 (1996).
[6] V. N. Dolgunin and A. A. Ukolov, ''Segregation modeling of particle rapid gravity flow,'' Powder Technol. **83**, 95–103 (1995).
[7] V. N. Dolgunin, A. N. Kudy, and A. A. Ukolov, ''Development of the model of segregation of particles undergoing granular flow down an inclined plane,'' Powder Technol. **96**, 211–218 (1998).
[8] J. J. McCarthy and J. M. Ottino, ''Particle dynamics simulation: A hybrid technique applied to granular mixing,'' Powder Technol. **97**, 91–99 (1998).
[9] P. W. Cleary, G. Metcalfe, and K. Liffman, ''How well do discrete element granular flow models capture the essentials of mixing processes?'' Appl. Math. Modeling **22**, 995–1008 (1998).
[10] P. K. Haff, ''Grain flows as a fluid mechanical phenomenon,'' J. Fluid Mech. **134**, 401–430 (1983).
[11] C. K. K. Lun, S. B. Savage, D. J. Jeffrey, and N. Chepurniy, ''Kinetic theories for granular flow: Inelastic particles in Couette flow and slightly inelastic particles in a general flow field,'' J. Fluid Mech. **140**, 223–256 (1984).
[12] P. C. Johnson and J. Jackson, ''Frictional-collisional constitutive equations for granular materials with application to plane shearing,'' J. Fluid Mech. **176**, 67–85 (1987); P. C. Johnson, P. Nott, and R. Jackson, ''Frictional-collisional constitutive equations of motion for particulate flows and their application to chutes,'' *ibid.* **210**, 501–511 (1990).
[13] K. M. Hill, J. F. Gilchrist, D. V. Khakhar, J. J. McCarthy, and J. M. Ottino, ''Mixing of granular materials: A test-bed dynamical system for pattern formation,'' Int. J. Bifurc. Chaos (to be published, 1999); J. M. Ottino and D. V. Khakhar, ''Mixing and segregation of granuler materials,'' Annu. Revs. Fluid Mech. (to be published, 2000).
[14] D. V. Khakhar, J. J. McCarthy, and J. M. Ottino, ''Radial segregation of materials in rotating cylinders,'' Phys. Fluids **9**, 3600–3614 (1997).
[15] N. Nityanand, B. Manley, and H. Henein, ''An analysis of radial segregation for different sized spherical solids in rotary cylinders,'' Metall. Trans. B **17B**, 247–257 (1986).
[16] G. H. Ristow, ''Particle mass segregation in a two-dimensional rotating drum,'' Europhys. Lett. **28**, 97–101 (1994); C. M. Dury and G. H. Ristow, ''Radial segregation in a two-dimensional rotating drum,'' J. Phys. I **7**, 737–745 (1997).
[17] F. Cantelaube and D. Bideau, ''Radial segregation in a 2D drum: Experimental analysis,'' Europhys. Lett. **30**, 133–138 (1995).
[18] E. Clement, J. Rajchenbach, and J. Duran, ''Mixing of a granular material in a bi-dimensional rotating drum,'' Europhys. Lett. **30**, 7–12 (1995).
[19] G. Baumann, I. M. Janosi, and D. E. Wolf, ''Surface properties and flow of granular material in a two dimensional rotating drum,'' Phys. Rev. E **51**, 1879–1888 (1995).
[20] L. Prigozhin and H. Kalman, ''Radial mixing and segregation of a binary mixture in a rotating drum: Model and experiment,'' Phys. Rev. E **57**, 2073–2080 (1998).
[21] M. L. de Haro, E. G. D. Cohen, and J. M. Kincaid, ''The Enskog theory for multicomponent mixtures. I. Linear transport theory,'' J. Chem. Phys. **78**, 2746–2759 (1983).
[22] J. M. Kincaid, E. G. D. Cohen, and M. L. de Haro, ''The Enskog theory for multicomponent mixtures. IV. Thermal diffusion,'' J. Chem. Phys. **86**, 963–975 (1987).
[23] J. T. Jenkins and F. Mancini, ''Kinetic theory for binary mixtures of smooth, nearly elastic spheres,'' Phys. Fluids A **1**, 2050–2057 (1989).
[24] B. Ö. Arnarson and J. T. Willits, ''Thermal diffusion in binary mixtures of

smooth, nearly elastic spheres with and without gravity,'' Phys. Fluids **10**, 1324–1328 (1998).
[25] D. Hirschfeld and D. C. Rapaport, ''Molecular dynamics studies of grain segregation in a sheared flow,'' Phys. Rev. E **56**, 2012–2018 (1997).
[26] G. A. Mansoori, N. F. Carnahan, K. E. Starling, and T. W. Leland, ''Equilibrium properties of the mixture of hard spheres,'' J. Chem. Phys. **54**, 1523–1525 (1971).
[27] T. M. Reed and K. E. Gubbins, *Applied Statistical Mechanics* (McGraw–Hill, New York, 1973), Chap. 6.
[28] J. T. Jenkins and M. W. Richman, ''Boundary conditions for plane flows of smooth nearly elastic circular discs,'' J. Fluid Mech. **71**, 53–69 (1986).
[29] J. O. Hirschfelder, C. F. Curtiss, and R. B. Bird, *Molecular Theory of Gases and Liquids* (Wiley, New York, 1954), Chap. 8.
[30] R. B. Bird, W. E. Stewart and E. N. Lightfoot, *Transport Phenomena* (Wiley, New York, 1960).
[31] J. Schafer, S. Dippel, and D. E. Wolf, ''Force schemes in simulations of granular materials,'' J. Phys. I **67**, 1751–1776 (1991).
[32] R. D. Mindlin, ''Compliance of elastic bodies in contact,'' J. Appl. Mech. **16**, 256–270 (1949).
[33] G. Ciccotti, D. Frenkel, and I. R. McDonald, *Simulation of Liquids and Solids* (North-Holland, Amsterdam, 1987), p. 82.